Solar Energy Materials & Solar Cells 266 (2024) 112677

Contents lists available at ScienceDirect

Solar Energy Materials and Solar Cells

journal homepage: www.elsevier.com/locate/solmat

Intercomparison of opto-thermal spectral measurements for concentrating solar thermal receiver materials from room temperature up to 800 °C

Simon Caron [a,*], Meryem Farchado [b], Gema San Vicente [b], Angel Morales [b], Jesus Ballestrín [c], Maria Joao Carvalho [d], Soraia Pascoa [d], Estelle le Baron [e], Angela Disdier [e], Emmanuel Guillot [f], Christophe Escape [f], Jean-Louis Sans [f], Yaniv Binyamin [g], Mubeen Baidossi [g], Florian Sutter [a], Marc Röger [a], Francisco Manzano-Agugliaro [h]

[a] Institute for Solar Research, German Aerospace Center (DLR), Calle Doctor Carracido 44-1, 04005, Almería, Spain
[b] CIEMAT-PSA, Plataforma Solar de Almería, Materials for Concentrating Solar Thermal Technologies Unit, Avenida Complutense 40, Madrid, 28040, Spain
[c] CIEMAT-PSA, Plataforma Solar de Almería, Carretera de Senés km. 4.5, Tabernas, 04200, Spain
[d] Laboratório Nacional de Energia e Geologia, I.P. (LNEG), Estrada do Paço do Lumiar, 22, 1649-038, Lisboa, Portugal
[e] Univ. Grenoble Alpes, CEA, Liten, LITEN, DTCH, L2TS, F-38000, Grenoble, France
[f] PROMES-CNRS, 7 rue du Four Solaire, Font Romeu, 66120, France
[g] Brightsource, 11 Kiryat Mada St., Amot Building n°6, P.O. Box 45220, Har Hotzvim, 91450, Jerusalem, Israel
[h] Department of Engineering, CEIA3, University of Almería, 04120, Almería, Spain

ARTICLE INFO

Keywords:
Concentrated solar power
Solar thermal
Absorber coating
Solar absorptance
Thermal emittance

ABSTRACT

An intercomparison of opto-thermal spectral measurements has been performed for some relevant receiver materials in concentrating solar thermal applications, from room temperature up to 800°C. Five European laboratories performed spectral measurements at room temperature, while two laboratories performed infrared spectral measurements at operating temperature up to 800 °C. Relevant materials include Haynes 230 (oxidized, Pyromark 2500 and industrial black coating) and silicon carbide. Two key figures of merit were analyzed: i) solar absorptance α_{sol} at room temperature, over the spectral range [0.3 – 2.5] μm, ii) thermal emittance $\varepsilon_{th}(T)$, over the common spectral range [2-14] μm, derived from spectral measurements performed from room temperature up to 800 °C.

Oxidized H230 reached an α_{sol} value of 90.9±1.0%. Pyromark 2500 reached an α_{sol} value of 96.3±0.5%, while the industrial black coating achieved an α_{sol} value of 97.0±0.4%. Silicon carbide reached an α_{sol} value of 93.5 ±1.1%. Low standard deviations in α_{sol} indicate reproducible measurements at room temperature.

For oxidized H230, the $\varepsilon_{th,calc}(T)$ value varied from 55% at room temperature up to 81% at 800 °C. For Pyromark 2500 and the industrial black coating, $\varepsilon_{th,calc}(T)$ fluctuated between 90% and 95%, with a weak temperature dependence. For silicon carbide, $\varepsilon_{th,calc}(T)$ varied from 70% at room temperature up to 86% at 800 °C. The typical standard deviation among participating laboratories is about 3%. $\varepsilon_{th,meas}(T)$ values derived from spectral measurements at operating temperature were consistent within a few percentage points in comparison to $\varepsilon_{th,calc}(T)$ values derived from spectral measurements at room temperature.

1. Introduction

Solar energy is a key player in the ongoing global energy transition towards decarbonization [1]. Concentrated Solar Thermal (CST) technology [2,3] could provide solar heat for a variety of industrial processes, especially high temperature processes above 400 °C, which may be difficult to electrify. CST technology combines a mirror field coupled to a thermal receiver to convert direct sunlight into useful heat. The thermal receiver is a key component, which absorbs solar power concentrated by the mirror field and transfers it to a heat transfer fluid (HTF). Two configurations exist, i.e. line focusing systems such as parabolic troughs and point focusing systems, such as Central Receiver Systems (CRS) [4–6].

The opto-thermal performance and durability of receiver materials and coatings is of particular importance [7–9]. Two key figures of merit,

* Corresponding author.
E-mail address: simon.caron@dlr.de (S. Caron).

https://doi.org/10.1016/j.solmat.2023.112677
Received 4 September 2023; Received in revised form 24 November 2023; Accepted 4 December 2023
Available online 11 December 2023

Nomenclature

Abbreviations

AM	Air Mass
ASTM	American Society for Testing Materials
CRS	Central Receiver System
CST	Concentrating Solar Thermal
DNI	Direct Normal Irradiance
DTGS	Deuterated Triglycine Sulfate
FT-IR	Fourier Transform Infrared
HTF	Heat Transfer Fluid
IR	Infrared
ISO	International Organization for Standardization
MCT	Mercury Cadmium Telluride
NIR	Near Infrared
OT	Operating Temperature
RT	Room Temperature
SDHR	Spectral Directional Hemispherical Reflectance
UV	Ultraviolet
VIS	Visible

Participants

CEA	Commissariat à l'énergie atomique et aux énergies alternatives
CIEMAT	Centro de Investigaciones Energéticas, Medioambientales y Tecnológicas
CNRS	Centre National de la Recherche Scientifique
DLR	Deutsches Zentrum für Luft- und Raumfahrt
MEDIASE	Moyens d'Essais et de Diagnostic pour l'Espace et l'Energie
OPAC	Joint CIEMAT-DLR optical laboratory at PSA
PROMES	Procédés et Matériaux pour l'Energie Solaire
PSA	Plataforma Solar de Almeria
LNEG	Laboratório Nacional de Energia e Geologia

English symbols

CV	Coefficient of variation [−]
$f_{\sigma T^4}$	Blackbody fraction [%]
I	Intensity [−]
L	Radiance [$W.m^{-2}.sr^{-1}$]
T	temperature [°C]
Z	Z-score [−]

Greek symbols

α	Absorptance [%]
ε	Emittance [%]
λ	Wavelength [μm]
ρ	Reflectance [%]
τ	Transmittance [%]
θ	Incidence angle [°]

Physical constants

c	Speed of light in vacuum [$m.s^{-1}$]
h	Planck's constant [J.s]
k	Boltzmann's constant [$J.K^{-1}$]
σ	Stefan-Boltzmann constant [$W.m^2.K^{-4}$]

English subscripts

base	Baseline
BB	Blackbody
calib	calibration
env	Ambient environment
meas	Measurement
sample	Sample
solar	Solar
th	Thermal
zero	Zeroline

i.e. solar absorptance α_{sol} and thermal emittance ε_{th} are considered for the characterization of such materials [10]. These figures are most often calculated on the basis of room temperature (RT) optical measurements performed with laboratory spectrophotometers [11,12]. Such spectral measurements have also been performed on some relevant receiver materials and coatings at operating temperature up to 800 °C (OT) [13–16].

Spectral emittance datasets at RT and OT are not only important for the evaluation and comparison of materials, but also for the design, calibration and operation of radiometric instrumentation, such as infrared thermography [17,18]. The following questions are relevant for scientists and engineers:

i) are significant deviations observed for figures of merit derived from RT and OT spectral measurements?
ii) Does the material exhibit a grey or a selective behavior in certain spectral ranges?
iii) Are local spectral shifts observed at higher temperature, outside of known atmospheric absorption bands?
iv) Does the emittance vary with the angular incidence of measurement at OT?

This paper focuses on the intercomparison of spectral emittance datasets for relevant materials in CRS applications. Substrates include nickel-chromium based superalloys (Haynes 230, short H230) [19] and Silicion Carbide (SiC) [20,21]. H230 samples are either oxidized or coated with black paints, such as Pyromark 2500 [22–26] or an industrial black coating provided by Brightsource Energy. Spectral emittance is measured and compared between five different laboratories, first at RT. Two laboratories (CEA, CNRS) further measure spectral emittance at OT, up to 800 °C, with three complimentary experimental setups.

The first section of this paper describes materials and methods, i.e. test campaign organization, reference materials, laboratory instrumentation and data processing. The second section covers the analysis and comparison of available experimental results at RT and OT.

2. Materials and methods

2.1. Organization and participants

This test campaign involved five research centres (CEA, CIEMAT, CNRS, DLR, LNEG), which laboratories are located in three European countries (France, Portugal, Spain). Participants and their role are described in Table 1. H230 samples were sequentially measured by each laboratory at RT, then submitted to CEA and CNRS for independent measurements at OT. SiC samples were measured independently by each laboratory. CIEMAT Madrid was included in this test campaign upon the completion of OT spectral measurements.

2.2. Reference samples

Eighteen H230 flat sample coupons were prepared for the RT and OT test campaigns. These coupons are described in Table 2 and are shown in Fig. 1 a). This sample lot is divided in three batches: i) oxidized H230, ii) Pyromark 2500 and iii) an industrial black coating. For each batch, three geometries were prepared (rectangular, disk, square inch), to comply

Table 1
Test campaign participants and roles.

Participant	Location	Role	Campaigns
CEA	Bourget-du-Lac, France	Measurements	RR-RT RR-OT (x1)
CIEMAT Madrid	Madrid, Spain	Measurements (a posteriori)	RR-RT
CIEMAT-PSA	Tabernas, Spain	Sample preparation (SiC)	[−]
CIEMAT-DLR (OPAC)	Tabernas, Spain	Measurements (initial)	RR-RT
PROMES-CNRS	Odeillo, France	Measurements	RR-RT
	Perpignan, France	Sample preparation (cutting)	RR-OT (x2)
DLR	Almería, Spain	Sample preparation (H230) Campaign coordination Data curation, evaluation	[−]
LNEG	Lisbon, Portugal	Measurements	RR-RT

with specifications for OT measurements. For each geometry, two duplicates were prepared and samples were previously exposed in a muffle furnace up to 800 °C before starting the test campaign. A subset of SiC sample coupons is shown in Fig. 1 b). Square samples (50x50 mm, 5 mm thickness) were originally submitted for RT and OT measurements. Without appropriate machining, OT measurements could only be satisfactorily performed by PROMES-CNRS laboratory up to 500 °C.

2.3. Instrumentation

2.3.1. RT measurements

2.3.1.1. Laboratory spectrophotometers. For RT measurements, spectral measurements are carried out from ultraviolet (UV) up to infrared (IR) wavelengths. This requires each participating laboratory to combine spectral measurements from two complementary spectrophotometers. Some laboratory spectrophotometers and integrating sphere geometries are illustrated in Fig. 2. An inventory of instrumentation is described in Table 3, while some spectrophotometer characteristics are listed in Table 4. Spectral ranges and raw dataset resolutions are summarized in Table 5.

In the UV, visible and near IR (UV-VIS-NIR), all laboratories used similar instrumentation, i.e. a Perkin Elmer Lambda 950 or 1050 spectrophotometer, with a white Ba_2SO_4 coated integrating sphere of diameter 150 mm. The light source incidence angle on the sample is near normal ($\Theta = 8°$). In the IR spectral range, all laboratories use a Fourier Transform (FT-IR) spectrophotometer. There are however diverse models, i.e. Perkin Elmer Frontier, Bruker Vertex 70 and Nicolet 6700. All participants except PROMES-CNRS use a Pike Ltd Mid-IR gold diffuse coated integrating sphere of diameter 76.2 mm. The light source incidence angle on the sample is also near normal ($\Theta = 12°$). PROMES-CNRS used the SOC 100 HDR hemi-ellipsoid coated with specular gold, for which the light source incidence angle is adjustable from 8 to 80° and set to 8° for these measurements.

For each participant, there is a partial spectral overlap between UV-VIS-NIR and FT-IR datasets, at least from 2 to 2.5 μm. A spectral mismatch may be induced during measurements, hypothetically explained by different instrument configurations (integrating sphere, detector type, calibration procedure). This mismatch should be ideally minimal for any sample.

Table 2
H230 flat sample coupons for RT and OT campaigns. All samples have a thickness of 2 mm.

Sample ID	Geometry	Coating	Surface preparation	Coating application	Thermal treatment
R01A/R01B	Rectangle, 45x50 mm	Uncoated	Sand blasted	N.A.	Oxidation 100 h at 800 °C
D01A/D01B	Disk, Ø 40 mm		Sand blasted		
A1/A2	Square, side length 25.4 mm		Sand blasted		
R02A/R02B	Rectangle, 45x50 mm	Pyromark 2500	Sand blasted	Workshop, Spray gun	Curing: 2h at 250 °C
D02A/D02B	Disk,Ø 40 mm		Sand blasted		2h at 540 °C
B1/B2	Square, side length 25.4 mm		Sand blasted		Pre-aging: 100h at 800 °C
S1/S2	Rectangle, 45x50 mm	Industrial, black	Sand blasted	External, proprietary	External, proprietary
S3/S4	Disk, Ø 40 mm		Sand blasted		
S5/S6	Square, side length 25.4 mm		Sand blasted		

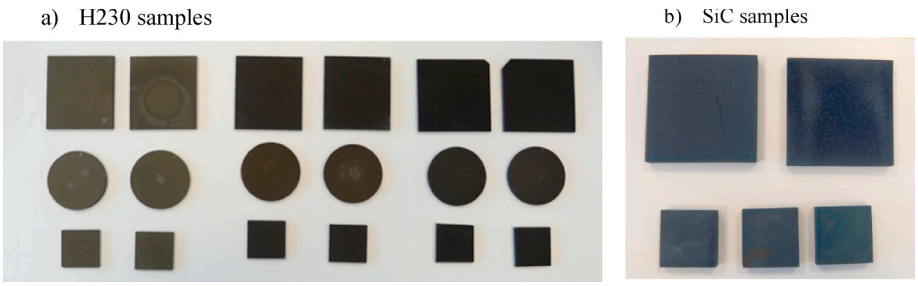

Fig. 1. a) H230 sample coupons submitted for RT and OT measurements. Samples are shown upon return after both RT and OT test campaigns. Top, from left to right: R01A, R01B, R02A, R02B, S1, S2. Middle, left to right: D01A, D01B, D02A, D02B, S3, S4. Bottom, left to right: A1, A2, B1, B2, S5, S6. b) SiC samples submitted for RT and OT measurements. Top: original samples. Bottom: Square inch samples cut by PROMES-CNRS for OT measurements up to 500 °C.

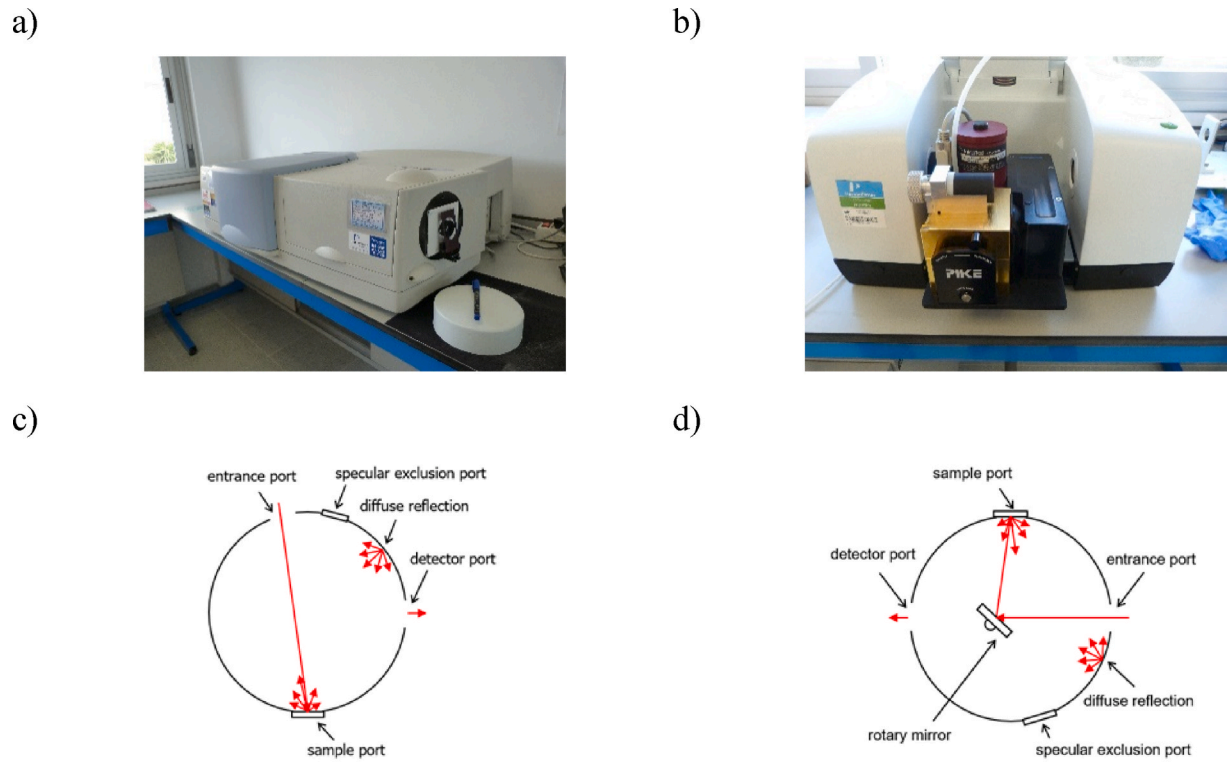

Fig. 2. a) Perkin Elmer Lambda 1050 spectrophotometer. b) Perkin Elmer Frontier FT-IR with Pike Ltd Mid-IR downward looking integrating sphere. c) Geometrical configuration for the Lambda 950/1050 integrating sphere. d) Geometrical configuration for the Pike Ltd mid-IR integrating sphere.

Table 3
Inventory of spectrophotometer for RT measurements.

Participant	UV-VIS-NIR (≤ 2.5 μm)		Infrared (> 1.5 μm)	
	Instrument	Integrating sphere	Instrument	Integrating sphere
CEA	Perkin Elmer Lambda 950	Perkin Elmer White diffuse Ø: 150 mm, Θ: 8°	Bruker Vertex 70 FT-IR	Pike Ltd Mid-IR Gold diffuse Ø: 76.2 mm, Θ: 12°
CIEMAT Madrid	Perkin Elmer Lambda 950	Perkin Elmer White diffuse Ø: 150 mm, Θ: 8°	Perkin Elmer Frontier FT-IR	Pike Ltd Mid-IR Gold diffuse Ø: 76.2 mm, Θ: 12°
CIEMAT-DLR (OPAC)	Perkin Elmer Lambda 1050	Perkin Elmer White diffuse Ø: 150 mm, Θ: 8°	Perkin Elmer Frontier FT-IR	Pike Ltd Mid-IR Gold diffuse Ø: 76.2 mm,Θ: 12°
PROMES-CNRS	Perkin Elmer Lambda 950	Perkin Elmer White diffuse Ø: 150 mm, Θ: 8°	Nicolet 6700 FT-IR	SOC 100 HDR Specular gold Hemiellipsoid Θ: 8°, Range: 8–80°
LNEG	Perkin Elmer Lambda 950	Perkin Elmer White diffuse Ø 150 mm, Θ: 8°	Perkin Elmer Frontier FT-IR	Pike Ltd Mid-IR Gold diffuse Ø 76.2 mm, Θ: 12°

Table 4
Overview of spectrophotometer characteristics.

Participant	UV-VIS-NIR (≤ 2.5 μm)		Infrared (> 1.5 μm)	
	Light sources	*Detectors (PMT)*	*Light sources*	*Detectors*
CEA	UV: Deuterium (^{2}H); VIS-IR: Tungsten (W)	InGaAs & PbS Peltier cooling	IR filament	MCT LN_2 cooling
CIEMAT Madrid	UV: Deuterium (^{2}H); VIS-IR: Tungsten (W)	InGaAs & PbS Peltier cooling	IR filament	MCT LN_2 cooling
CIEMAT-DLR (OPAC)	UV: Deuterium (^{2}H); VIS-IR: Tungsten (W)	InGaAs & PbS Peltier cooling	IR filament	MCT LN_2 cooling
PROMES-CNRS	UV: Deuterium (^{2}H); VIS-IR: Tungsten (W)	InGaAs & PbS Peltier cooling	Blackbody (700 °C)	InGaAs & DTGS Peltier cooling
LNEG	UV: Deuterium (^{2}H); VIS-IR: Tungsten (W)	InGaAs & PbS Peltier cooling	IR filament	DTGS without cooling

2.3.1.2. Baseline coupons. An inventory of flat baseline coupons is provided in Table 6, while typical reflectance spectra are shown in Fig. 3. These baseline coupons are used as reference for the calibration of spectral datasets. All participants expect CIEMAT-DLR (OPAC) used a white diffuse flat coupon (Spectralon, 99% reflectance) for UV-VIS-NIR measurements while a gold diffuse (Infragold, ~94% reflectance) or gold specular flat coupon is used for FT-IR measurements. These coupons are traceable to primary standards. CIEMAT-DLR used custom secondary standards, i.e. a black coated sample for UV-VIS-NIR and a black or solar selective coupon for FT-IR measurements. These secondary standards were calibrated by OMT Solutions, Netherlands [11].

The selection of a baseline is a subjective decision made by the operator, depending on the sample to be measured. An empirical rule of thumb consists in selecting a baseline "similar" to the sample to be measured. If the baseline has a flat spectral response, it may be suitable for a broader range of materials, while custom secondary standards are more prone to induce spectral mismatches.

Table 5
Spectral ranges and sampling resolutions of raw datasets.

Participant	UV-VIS-NIR (≤2500 nm)		Infrared (>1500 nm)	
	Spectral range [μm]	*Spectral resolution [nm]*	*Spectral range [μm]*	*Spectral resolution [nm]*
CEA	0.28 to 2.5 μm	5 nm	1.8 – 16 μm	10 nm
CIEMAT Madrid	0.28 – 2.5 μm	10 nm	2 – 17 μm	~2 nm
CIEMAT-DLR (OPAC)	0.28 – 2.5 μm	5 nm	2 – 16 μm	4 nm
PROMES-CNRS	0.25 – 2.5 μm	5 nm	1.5 – 26 μm	variable
LNEG	0.3 – 2.5 μm	5 nm	2 – 16 μm	16 or 20 nm

Table 6
Baseline flat reference coupons used for calibration.

Participant	UV-VIS-NIR (≤ 2.5 μm)	Infrared (> 1.5 μm)
	Baseline	Baseline
CEA	White diffuse, Spectralon 99%, certified yearly at LNE, France	Gold diffuse, Infragold certified yearly at LNE, France
CIEMAT Madrid	White diffuse, Spectralon 99% Labsphere calibration	Gold diffuse, Infragold
CIEMAT-DLR (OPAC)	Black (secondary standard, OMT)	Black (secondary standard, OMT) Selective (secondary standard, OMT)
PROMES-CNRS	White diffuse, Spectralon 99% Labsphere calibration	Gold diffuse (Infragold) Specular gold, NIST traceable
LNEG	White diffuse, Spectralon 99% Labsphere calibration	Gold diffuse (Infragold), Avian Tech

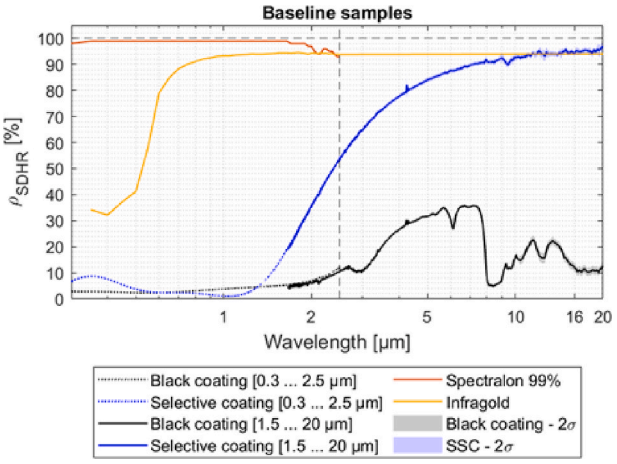

Fig. 3. Spectral directional hemispherical reflectance (SDHR) of flat baseline coupons.

Table 7
Temperature and spectral ranges for OT measurements.

Participant	Instrument	Temperature range	Spectral range
CEA	Bruker Vertex 70 FT-IR + IR 563/301 blackbody	200 to 800 °C	DTGS: 2 to 26 μm
PROMES-CNRS	Nicolet 6700 FT-IR + SOC 100 HDR	RT to 500 °C	InGaAs:1 to 2 μm DTGS: 2 to 26 μm
PROMES-CNRS	MEDIASE SR 5000 N spectroradiometer	~700 to 800 °C Tentative <700 °C	InSb + MCT (77 K): 1.34 to 14 μm

2.3.2. OT measurements

CEA and PROMES-CNRS performed OT measurements with independent experimental setups. Temperature and spectral ranges are summarized in Table 7.

2.3.2.1. CEA laboratory setup. CEA laboratory setup development is described in Ref. [27] and the equipment is shown in Fig. 4. This setup consists of a Bruker Vertex 70 FT-IR spectrophotometer, with a modified optical path, including a custom optical bench. This optical bench is mounted between the heated sample and a blackbody source IR 563/301 [28]. Inside the optical bench, a rotary parabolic mirror is alternatively switched towards the heated sample and the blackbody source. The sample holder integrates a thermal shield and a thermal control unit. The sample surface temperature T_{sample} is measured on its front side with six thermocouples.

The spectral emittance $\varepsilon(\lambda,T)$ of the sample is the ratio between the radiance of the sample $L_{sample}(\lambda,T)$ and the radiance of the blackbody $L_{BB}(\lambda,T)$ at the same temperature T. The response of the spectrophotometer is compared to the theoretical blackbody spectrum to determine a correction function for this instrument.

During OT measurements, the sample temperature could be controlled from 200 °C to 750 °C. The angle of incidence is set to 12°. The spectral range spans from 2 to 26 μm with a variable resolution.

2.3.2.2. PROMES-CNRS laboratory setup. PROMES-CNRS laboratory setup consists of a Nicolet 6700 FT-IR combined with the hemi-ellipsoid SOC 100 HDR. The sample is mounted on a sample holder, which includes a heater which can heat the sample from RT (25 °C) up to 500 °C. Two detectors are used for OT measurements: InGaAs (1 to 2 μm) and DTGS (2 to 26 μm). This measurement setup does not require a blackbody and there is no modification of the spectrophotometer optical path in comparison to RT measurements.

2.3.2.3. MEDIASE setup. The MEDIASE setup operated by PROMES-CNRS is shown in Fig. 5 and described in Refs. [19,20]. The sample is mounted at the focus of the 1 MW solar furnace and heated on its backside with concentrated solar radiation (up to 10 MW/m^2), through a hemispherical silica window. The disk sample is maintained in the water-cooled sample holder by three thin alumina needles placed every 120° around the sample circumference. The sample temperature is measured on the front side with a two-color pyro-reflectometer developed at PROMES-CNRS [29]. Given the very low reflectivity of tested materials, the temperature measurement by pyro-reflectometry was actually not possible. The sample temperature was thus measured by applying the two-color pyrometry technique with the installed two-color pyro-reflectometer. The setup is equipped with a turbo-molecular vacuum pump, which allows operating under vacuum conditions. During OT measurements, all experiments were performed under secondary vacuum at around 2.10^{-3} Pa.

The radiance measurements are carried out with a SR-5000 N spectroradiometer [30]. The spectroradiometer is equipped with an InSb – MCT sandwich detector cooled to 77 K with liquid nitrogen (LN_2), superseding a MCT detector cooled by Peltier effect to 213 K. Spectral measurements are carried out from 1.34 up to 14 μm. The spectral resolution increases stepwise from 13 nm (1.34 -2.55 μm) to 74 nm (8.4 to 14 μm). The distance between the sample and the spectroradiometer is 1 m. The spectroradiometer looks on the heated sample through a thallium-iodo-bromide (KRS5) window. Using an original three mirror goniometer system developed by PROMES-CNRS, spectral directional emittance measurements are obtained for several incidence angles, i.e. from 0° to 80°, in steps of 10°, as well as 45° and 75°. The spectroradiometer-goniometer optical assembly and the pyro-reflectometer were calibrated before the test campaign, in front of a blackbody which temperature is measured with a standard pyrometer.

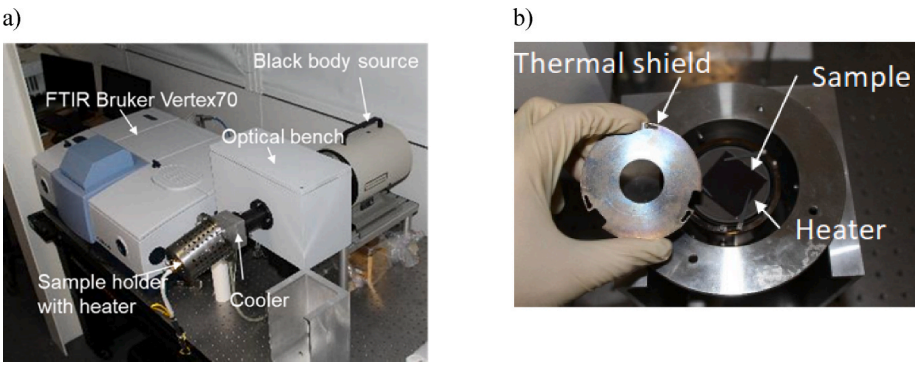

Fig. 4. CEA laboratory setup for spectral emittance measurements at operating temperature. a) Benchtop optical assembly. b) Sample holder overview.

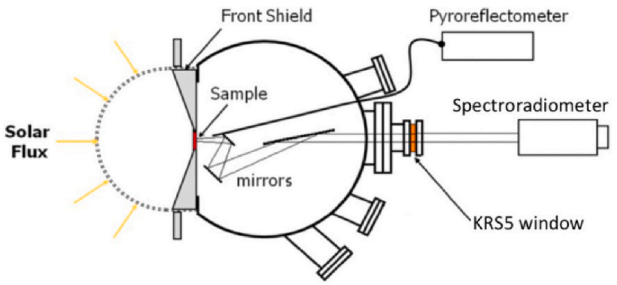

Fig. 5. MEDIASE setup mounted at the focus of the 1 MW solar furnace in Odeillo, France.

2.4. Data processing

2.4.1. Data curation

A common spectral range is defined for the calculation of figures of merit: α_{sol} and ε_{th}. The common UV-VIS-NIR spectral range spans from 0.3 μm to 2.5 μm, while the common spectral range for IR measurements spans from 2 μm to 14 μm, according to Tables 5 and 7. Both spectral ranges overlap from 2 μm to 2.5 μm. The spectral resolution is set to 5 nm by linear interpolation of spectral datasets.

2.4.2. Reflectance measurements

For all RT and OT reflectance measurements, the sample SDHR ($\rho_{sample,SDHR}$) is calculated with a set of spectrophotometer measurements according to (Eq. (1)). First the sample port is left empty for a zeroline or background measurement ($I_{zero,\ meas}$). A baseline coupon is then measured ($I_{base,\ meas}$). Its reference calibration data is referred as $\rho_{base,calib}$. The sample coupon is then measured after its temperature is stabilized to the desired setpoint ($I_{sample,\ meas}$).

$$\rho_{sample,SDHR}(\lambda,\theta,T) = \frac{I_{sample,meas}(\lambda,\theta,T) - I_{zero,meas}(\lambda,\theta,RT)}{I_{base,meas}(\lambda,\theta,RT) - I_{zero,meas}(\lambda,\theta,RT)} \cdot \rho_{base,calib} \quad (1)$$

Assuming opaque samples, the spectral absorptance and spectral emittance are derived according to Kirchhoff's law of thermal radiation (Eq. (2)):

$$\alpha(\lambda) = 1 - \rho(\lambda); \alpha(\lambda) = \varepsilon(\lambda) \quad (2)$$

2.4.3. Radiance measurements

For OT measurements involving a blackbody reference, the sample radiance L_{sample} is measured instead of its reflectance. CEA setup involves a direct comparison with a blackbody reference during the measurement, while MEDIASE setup involves a comparison with an a priori radiometric calibration of the spectroradiometer under laboratory conditions.

2.4.3.1. CEA setup. The spectrophotometer measures the radiance of the hot sample but also the luminance reflected by the surrounding environment. The measured signal L*(λ,T) is the sum of two radiance terms (Eq. (3)).

$$L^*(\lambda,T) = \varepsilon(\lambda,T_{sample}).L_{BB}(\lambda,T_{sample}) + \left[1 - \varepsilon(\lambda,T_{sample})\right].L_{BB}(\lambda,T_{env}) \quad (3)$$

The spectral emittance $\boldsymbol{\varepsilon}(\lambda,T_{sample})$ of a sample is thus calculated according to (Eq. (4)):

$$\varepsilon(\lambda,T) = \frac{L^*(\lambda,T_{sample}) - L_{BB}(\lambda,T_{env})}{L_{BB}(\lambda,T_{sample}) - L_{BB}(\lambda,T_{env})} \quad (4)$$

2.4.3.2. MEDIASE setup. The spectroradiometer signal measures the spectral directional radiance of the heated sample $L_s(\lambda,\Theta,T)$. The spectral directional emittance ε (λ,Θ,T) is calculated according to (Eq. (5)), for measurements at temperature significantly higher than RT:

$$\varepsilon(\lambda,\Theta,T) = \frac{L_{sample}(\lambda,\Theta,T)\tau_{atm,sample}(\lambda,d=1\ m)}{L_{BB}(\lambda,T)\tau_{atm,BB}(\lambda,d=1\ m)} \quad (5)$$

If sample and blackbody measurements are performed in a short period of time, the effect of atmospheric spectral transmittance on the measurement would cancel out ($\tau_{atm,sample}/\tau_{atm,BB} \sim 1$). During OT measurements, this time interval varied from a few days to a few months. Local atmospheric absorption effects could be observed in some spectra, mainly due to water vapor and carbon dioxide. The most visible absorption bands are located around 1.37, 1.87, 2.7, 4.2 and 5.5-7.3 μm.

The spectral hemispherical emittance ε(λ,T) is calculated according to (Eq. (6)), assuming $\varepsilon(\Theta = 90°) = 0$:

$$\varepsilon(\lambda,T) = \int_0^{\pi/2} \varepsilon(\lambda,\Theta,T)\sin(2\theta)d\theta \quad (6)$$

2.4.4. Figures of merit

2.4.4.1. Solar absorptance. Solar absorptance α_{sol}(AM) is calculated for UV-VIS-NIR measurements at RT according to (Eq. (7)). G_{sol}(λ,AM) corresponds to the reference solar spectrum for a given Air Mass (AM). This spectrum is defined according to ASTM G173-03 [16], using SMARTS v2.9.2, for direct andcircumsolar radiation, setting AM to 1.5. The common UV-VIS-NIR spectral range is selected, i.e. $\lambda_1 = 0.3$ μm; $\lambda_2 = 2.5$ μm.

$$\alpha_{sol}(\mathrm{AM}) = \frac{\int_{\lambda_1}^{\lambda_2} \left[1 - \rho_{sample,SDHR}(\lambda,\theta,RT)\right].G_{sol}(\lambda,AM)d\lambda}{\int_{\lambda_1}^{\lambda_2} G_{sol}(\lambda.AM)d\lambda} \quad (7)$$

2.4.4.2. Thermal emittance. Thermal emittance $\varepsilon_{th}(T)$ is calculated from IR measurements at RT and OT according to (Eq. (8)). The common IR spectral range is defined for integration, i.e. $\lambda_3 = 2$ μm and $\lambda_4 = 14$ μm. FT-IR and radiance measurements are considered for this calculation.

$$\varepsilon_{th}(T) = \frac{\int_{\lambda_3}^{\lambda_4} \varepsilon(\lambda,T).L_{BB}(\lambda,T)d\lambda}{\int_{\lambda_3}^{\lambda_4} L_{BB}(\lambda,T)d\lambda} \quad (8)$$

L_{BB} corresponds to the blackbody radiance, calculated according to Planck's law (Eq.9):

$$L_{BB}(\lambda,T) = \frac{2\pi hc^2}{\lambda^5\left[exp\left(\frac{hc}{\lambda kT_{abs}}\right)-1\right]} \quad (9)$$

For RT measurements, $\varepsilon(\lambda,T)$ is assumed to remain constant at any temperature (Eq. (10)). The thermal emittance $\varepsilon_{th}(T)$ calculated according to (Eq. (8)) is labeled $\varepsilon_{th,calc}(T)$.

$$\frac{\partial\varepsilon(\lambda,T)}{\partial T} \backsim 0 \quad (10)$$

For OT measurements, $\varepsilon(\lambda,T)$ is directly measured, assuming there is no sample degradation at higher temperature. The thermal emittance $\varepsilon_{th}(T)$ is then labeled $\varepsilon_{th,meas}(T)$. The main objective of this paper is to observe whether there are significant deviations between $\varepsilon_{th.calc}(T)$ and $\varepsilon_{th,meas}(T)$ for selected materials (Eq. (11)).

$$\Delta\varepsilon(T) = \varepsilon_{th,meas}(T) - \varepsilon_{th,calc}(T) \quad (11)$$

It is worth observing that the common IR spectral range (2–14 μm) covers a fraction $f_{\sigma T^4}$ of the total blackbody radiance (Eq. (12)), where σ corresponds to Stefan-Boltzmann constant. The thermal emittance $\varepsilon_{th}(T)$ defined above (Eq. (8)) thus approximates the total thermal emittance $\varepsilon_{th}(T)$ of the reference surface.

$$f_{\sigma T^4} = \frac{\int_{\lambda_3}^{\lambda_4} E_{bb}(\lambda,T)d\lambda}{\int_0^{\infty} E_{bb}(\lambda,T)d\lambda} = \frac{\int_{\lambda_3}^{\lambda_4} E_{bb}(\lambda,T)d\lambda}{\sigma T^4} \quad (12)$$

The reference solar spectrum [31] is shown in Fig. 6 a) and compared to the blackbody spectral radiance at 25 °C and 800 °C. The fraction $f_{\sigma T^4}$ is shown for different spectral bands as a function of blackbody temperature in Fig. 6 b). At low temperature, the spectral overlap of the blackbody and the reference solar spectra is negligible (Fig. 6 a), while the spectral overlap below 2 μm is no longer negligible as the blackbody temperature increases.

The analysis of $f_{\sigma T^4}$ (Fig. 6 b) shows that the upper integration limit (14 … 50 μm) has a significant impact on the thermal emittance calculation (Eq. (8)) as the temperature decreases. The lower integration limit (0.3 … 2 μm) has a significant impact on the thermal emittance calculation as the temperature increases. The red curve (interval 0.3 … 14 μm) and dark blue curve (interval 2 … 14 μm) overlap within 1% from 25 °C to 450 °C, while the deviation increases at higher temperature levels. Consequently, ε_{th} values integrated from 2 to 14 μm are slightly underestimated in comparison to ε_{th} values integrated from 0.3 to 16 μm for the selected materials, above 500 °C. This deviation increases with temperature and its average value is estimated at 0.4% for 800 °C.

2.4.5. Statistical treatment

For each measured sample (j), a set of statistical indicators is computed for figures of merit α_{sol} and $\varepsilon_{th}(T)$ when applicable, from each participating laboratory (i). Following statistical indicators are calculated: i) Mean value μ_j, ii) Standard deviation σ_j iii) Coefficient of variation $CV_j = \sigma_j/\mu_j$, iv) the Z-score, defined according to ISO 13528:2015 [32] (Eq. (13)).

$$Z_{i,j} = \frac{x_{i,j} - \mu_j}{\sigma_j} \quad (13)$$

The Z-score $Z_{i,j}$ is calculated for each participating laboratory (i), considering the corresponding figure of merit $x_{i,j}$ for a given sample j. The Z-score is interpreted as follows:

- if |Z-score| <2, the comparison is satisfactory
- if 2<|Z-score|<3, the comparison is questionable
- if |Z-score| >3, the comparison is unsatisfactory

3. Results and discussion

3.1. Room temperature

3.1.1. Solar absorptance

Solar absorptance results for H230 and SiC sample coupons are summarized in Table 8 and shown in Fig. 7. Oxidized H230 sample

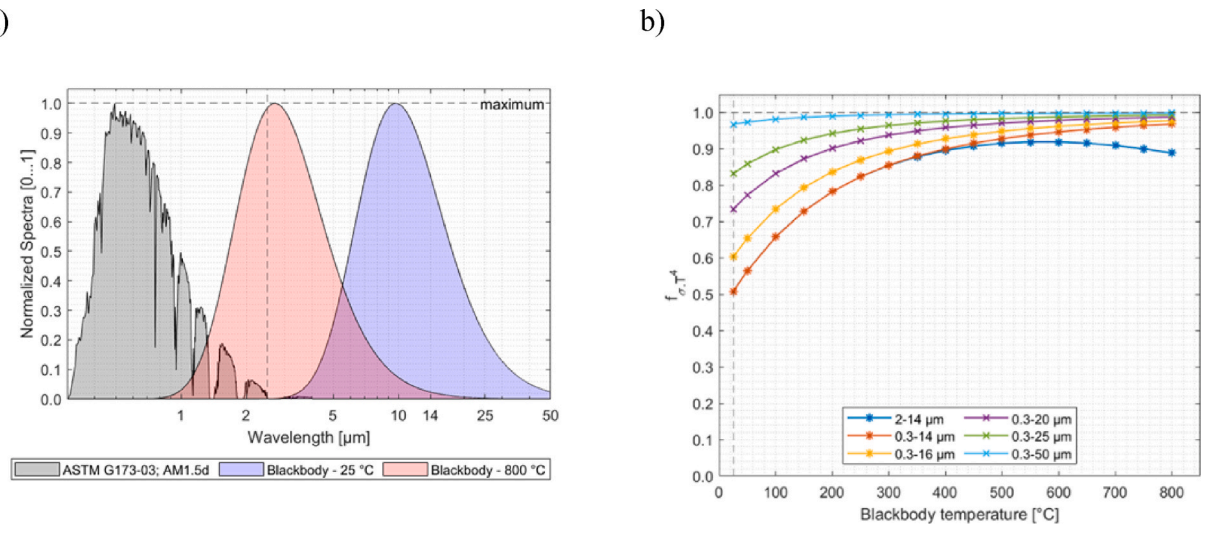

Fig. 6. a) Reference solar spectrum [31] and blackbody spectra at 25 and 800 °C. b) Fraction of Stefan-Boltzmann law ($f_{\sigma T^4}$) as a function of blackbody temperature for different spectral ranges.

Table 8
Summary of solar absorptance (α_{sol}) results for H230 and SiC samples at RT.

Sample	CEA	CIEMAT-DLR (OPAC)	PROMES-CNRS	LNEG	CIEMAT Madrid	Mean μ	Stdev σ	CV σ/μ
R01A	90.4%	88.9%	90.3%	91.5%	91.0%	90.4%	1.0%	1.1%
R01B	90.6%	89.1%	90.6%	91.6%	91.2%	90.6%	1.0%	1.1%
D01A	90.2%	88.1%	89.8%	91.0%	91.3%	90.1%	1.3%	1.4%
D01B	91.2%	89.9%	90.9%	92.1%	91.8%	91.2%	0.9%	1.0%
A1	91.4%	90.0%	91.1%	92.4%	91.6%	91.3%	0.9%	0.9%
A2	91.7%	90.4%	91.4%	92.6%	91.9%	91.6%	0.8%	0.9%
R02A	96.2%	96.7%	96.1%	96.7%	96.5%	96.4%	0.3%	0.3%
R02B	96.4%	96.9%	96.4%	96.8%	96.7%	96.6%	0.2%	0.2%
D02A	96.3%	96.8%	96.2%	96.8%	91.2%	95.5%	2.4%	2.5%
D02B	96.2%	96.7%	96.0%	96.6%	89.9%	95.1%	2.9%	3.1%
B1	96.0%	96.5%	95.9%	96.4%	95.6%	96.1%	0.4%	0.4%
B2	96.3%	96.7%	96.1%	96.7%	95.7%	96.3%	0.4%	0.4%
S1	97.1%	97.4%	97.0%	97.3%	97.7%	97.3%	0.3%	0.3%
S2	97.0%	97.4%	96.9%	97.3%	97.7%	97.3%	0.3%	0.3%
S3	97.0%	97.3%	97.0%	97.2%	93.9%	96.5%	1.5%	1.5%
S4	96.9%	97.3%	97.0%	97.2%	93.2%	96.3%	1.8%	1.8%
S5	96.7%	97.1%	96.6%	97.0%	96.6%	96.8%	0.3%	0.3%
S6	96.7%	97.2%	96.5%	97.0%	96.4%	96.7%	0.3%	0.3%
SiC	93.3%	94.2%	92.3%	93.6%	93.9%	93.5%	1.1%	1.2%

coupons reach an α_{sol} value of 90.9±1.0%. Meanwhile, Pyromark 2500 sample coupons reach an α_{sol} value of 96.3±0.5%, while the industrial grade black coating achieves an α_{sol} value of 97.0±0.4%. The low standard deviation indicates reproducible measurements over a quite homogeneous sample batch. Each participating laboratory performed spectral measurements on three spots. The typical standard deviation for α_{sol} due to coating inhomogeneity was less than 0.1%. For SiC samples, α_{sol} value reaches 93.5±1.1%. A slightly higher standard deviation is observed for SiC in comparison to black coated samples, probably explained by the initial sample batch slight inhomogeneity. All measurements lie within one standard deviation.

A few patterns can be identified analysing Z-scores in Fig. 7. For instance, CIEMAT-DLR (OPAC) laboratory tends to underestimate α_{sol} for oxidized H230 sample coupons (Z ~ -1.5). Measurements performed by CIEMAT Madrid after the OT test campaign tend to be consistent with previous measurements, except for a few flat disk samples which degraded during transport (D02A/D02B, S3/S4; Z: ~ -1.8). All Z-scores are lower than 2, the comparison is thus statistically satisfactory.

3.1.2. Thermal emittance

Thermal emittance results $\varepsilon_{th,calc}$ for H230 and SiC sample coupons are summarized in Table 9 and shown in Figs. 8 and 9. Values are reported at 800 °C for comparison.

Fig. 8 indicates how the mean $\varepsilon_{calc}(T)$ value varies with blackbody temperature for each H230 sample coupon. For oxidized H230 sample coupons, the $\varepsilon_{th,calc}$ value calculated from 2 to 14 μm varies from 55% at RT up to 85% at 1000 °C. For Pyromark 2500 and the industrial black coating, the $\varepsilon_{th,calc}$ value lies between 90% and 95%. For SiC samples, the $\varepsilon_{th,calc}$ value varies from 70% at RT up to 87% at 1000 °C. The typical standard deviation among participating laboratories is about 3%. A good homogeneity is observed for each group of sample coupons. Each participating laboratory performed spectral measurements on three spots. The typical standard deviation for ε_{th} due to coating inhomogeneity was less than 0.2%.

The Z-score is shown in Fig. 9 b), d) and f). It is worth observing that $\varepsilon_{th,calc}$ values obtained from CIEMAT Madrid are systematically lower in comparison to other participating laboratories, for any sample type (Z-score ~ -1.6). it is difficult to determine the exact origin of this deviation, i.e. if it is related to the instrumentation itself or to any sample degradation which may have occurred during measurements at operating temperature. Low spectral mismatches were observed for measurements in the overlap range (2 … 2.5 μm) for most participating laboratories, in particular for CEA and PROMES-CNRS (Δ < 1 p.p.). Higher spectral mismatches were noticed for CIEMAT Madrid. All absolute Z-score values are lower than 2, indicating a satisfactory comparison.

3.2. Operating temperature

H230 sample coupons could be measured at OT with all experimental setups, while SiC sample coupons could be only measured satisfactorily with PROMES-CNRS laboratory setup.

3.2.1. CEA laboratory setup

Spectral measurements for H230 sample coupons recorded from 220 °C to 760 °C by CEA are shown in Fig. 10. The spectral behaviour is consistent for each pair of sample coupons. These samples tend to exhibit stable optical spectra at OT, although weak temperature dependent spectral shifts are locally observed at short wavelengths (<3 μm) and lower temperatures. Significant noise can be observed in this case, yielding local spectral emittance values above 100%. Local artefacts caused by atmospheric absorption bands are also observed locally, distorting spectra around 2.7, 3.4, 4.2 and 5.7 μm.

Oxidized H230 sample coupons (R01A/R02B) exhibit a selective spectrum, i.e. their spectral emittance decreases from 90% to 50% over the recorded spectral range. Pyromark 2500 sample coupons (R02A/R02B) rather exhibit a grey spectral profile, their spectral emittance fluctuated above 90%. A similar behaviour is observed for the industrial black coating (S1/S2).

3.2.2. PROMES-CNRS laboratory setup

Spectral measurements for H230 sample coupons recorded by

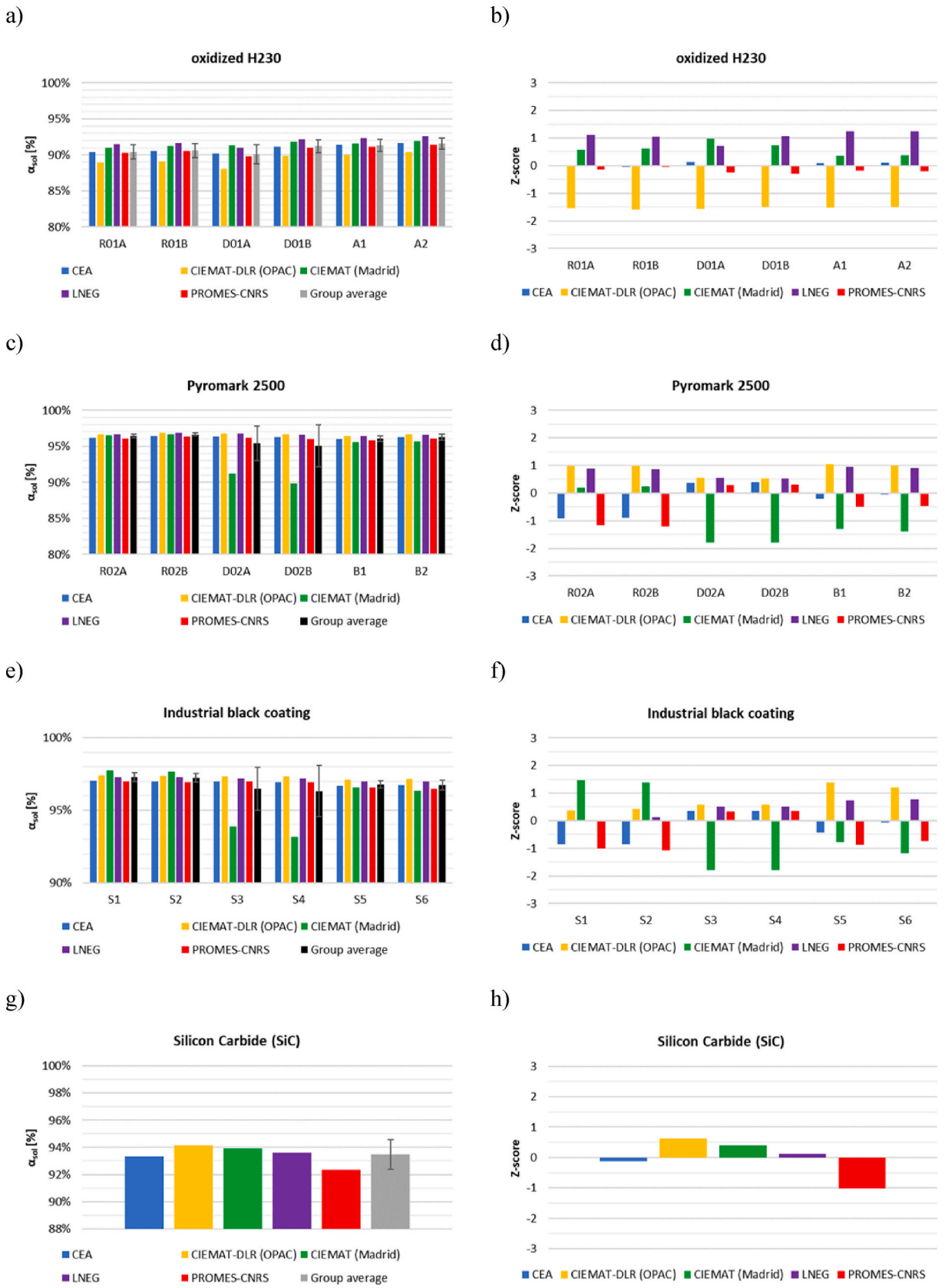

Fig. 7. Solar absorptance results α_{sol} for H230 sample coupons (RT measurements). a) oxidized H230, absolute values. b) oxidized H230, Z-score. c) Pyromark 2500, absolute values. d) Pyromark 2500, Z-score. e) Industrial black coating, absolute values. f) Industrial black coating, Z-score. g) SiC samples, absolute values. h) SiC samples, Z-score.

Table 9
Thermal emittance $\varepsilon_{th,calc}$ (800 °C) results for H230 sample coupons (RT measurements).

Sample	CEA	CIEMAT-DLR (OPAC)	PROMES-CNRS	LNEG	CIEMAT Madrid	Mean μ	Stdev σ	CV σ/μ
R01A	81.2%	80.1%	78.5%	82.8%	74.4%	79.2%	3.6%	4.5%
R01B	80.6%	80.5%	80.8%	84.3%	74.2%	79.9%	4.1%	5.1%
D01A	79.6%	78.8%	77.8%	78.8%	72.8%	77.3%	3.2%	4.2%
D01B	82.5%	82.7%	81.3%	82.8%	76.3%	81.0%	3.2%	3.9%
A1	81.8%	80.8%	80.1%	84.0%	76.4%	80.5%	2.9%	3.7%
A2	83.2%	83.2%	81.9%	85.5%	76.8%	81.9%	3.6%	4.4%
R02A	92.0%	94.1%	93.6%	94.8%	87.1%	92.3%	3.1%	3.4%
R02B	92.3%	94.6%	93.6%	95.2%	87.3%	92.6%	3.2%	3.5%
D02A	92.7%	94.7%	93.7%	93.8%	81.0%	91.3%	5.5%	6.0%
D02B	92.6%	94.5%	93.7%	94.9%	80.2%	91.3%	5.9%	6.5%
B1	92.3%	94.3%	93.2%	94.8%	86.8%	92.2%	3.2%	3.5%
B2	92.6%	94.6%	93.8%	94.9%	86.9%	92.6%	3.3%	3.6%
S1	91.8%	93.5%	93.5%	94.9%	87.4%	92.2%	2.9%	3.2%
S2	91.7%	93.6%	93.5%	94.8%	87.6%	92.2%	2.9%	3.1%
S3	91.9%	93.4%	93.5%	94.8%	82.1%	91.2%	5.1%	5.6%
S4	91.7%	93.0%	93.3%	95.1%	79.6%	90.6%	6.2%	6.8%
S5	93.4%	95.2%	95.4%	96.2%	89.3%	93.9%	2.8%	3.0%
S6	93.2%	94.9%	95.1%	96.1%	89.1%	93.7%	2.8%	3.0%
SiC	87.9%	84.6%	87.0%	88.3%	83.5%	86.2%	2.1%	2.5%

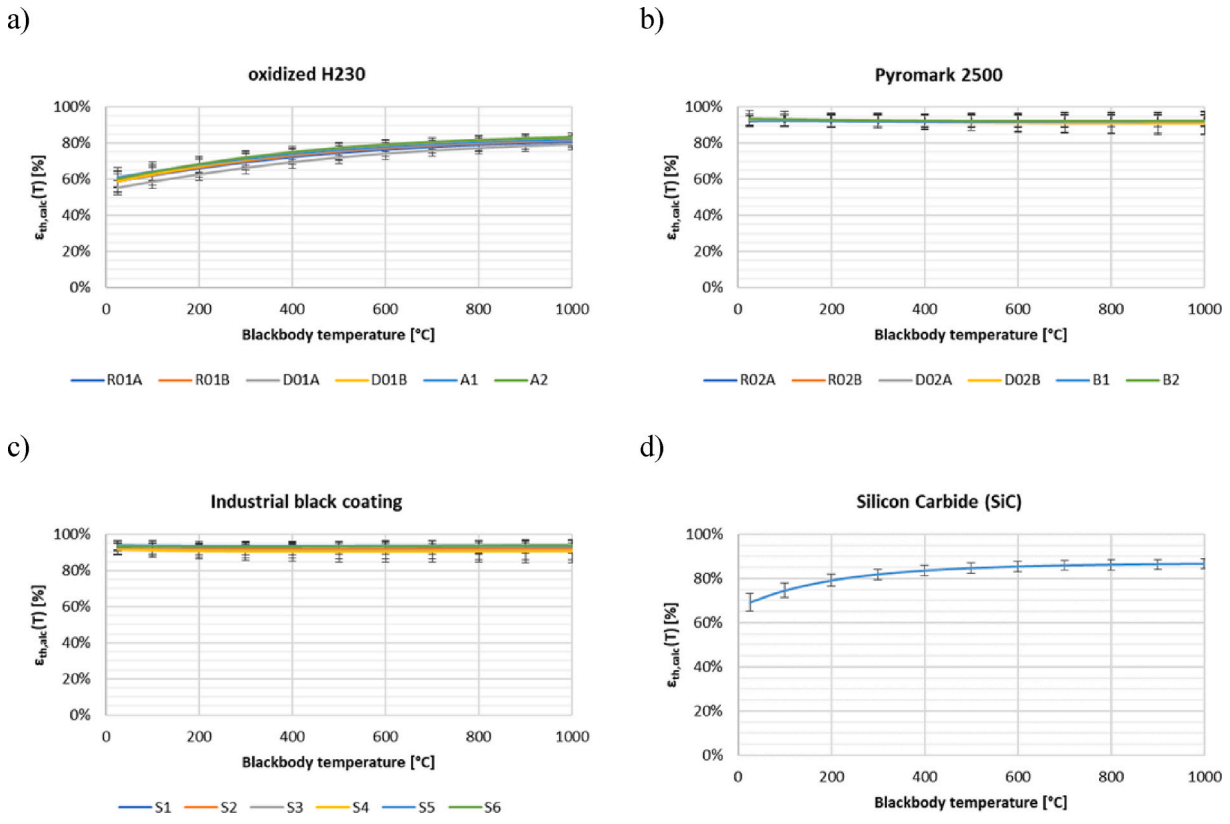

Fig. 8. Thermal emittance $\varepsilon_{th,calc}(T)$ for H230 and SiC sample coupons (RT measurements). a) oxidized H230, b) Pyromark 2500, c) Industrial black coating. d) SiC sample coupons.

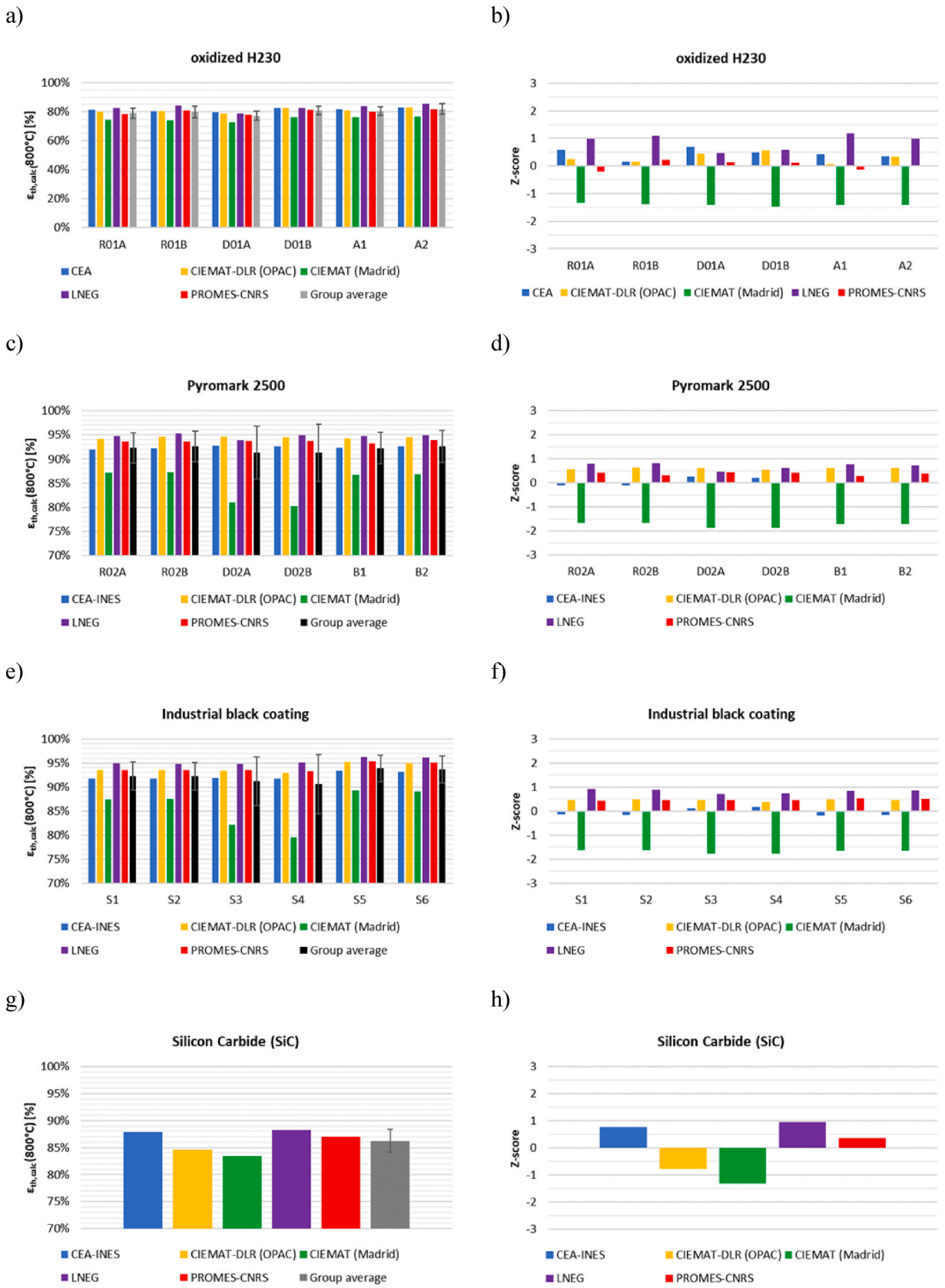

Fig. 9. Thermal emittance $\varepsilon_{th,calc}$(800 °C) for H230 and SiC samples measured at RT. a) oxidized H230, absolute values. b) oxidized H230, Z-score. c) Pyromark 2500, absolute values. d) Pyromark 2500, Z-score. e) Industrial black coating, absolute values. f) Industrial black coating, Z-score. f) SiC, absolute values. g) SiC, Z-score.

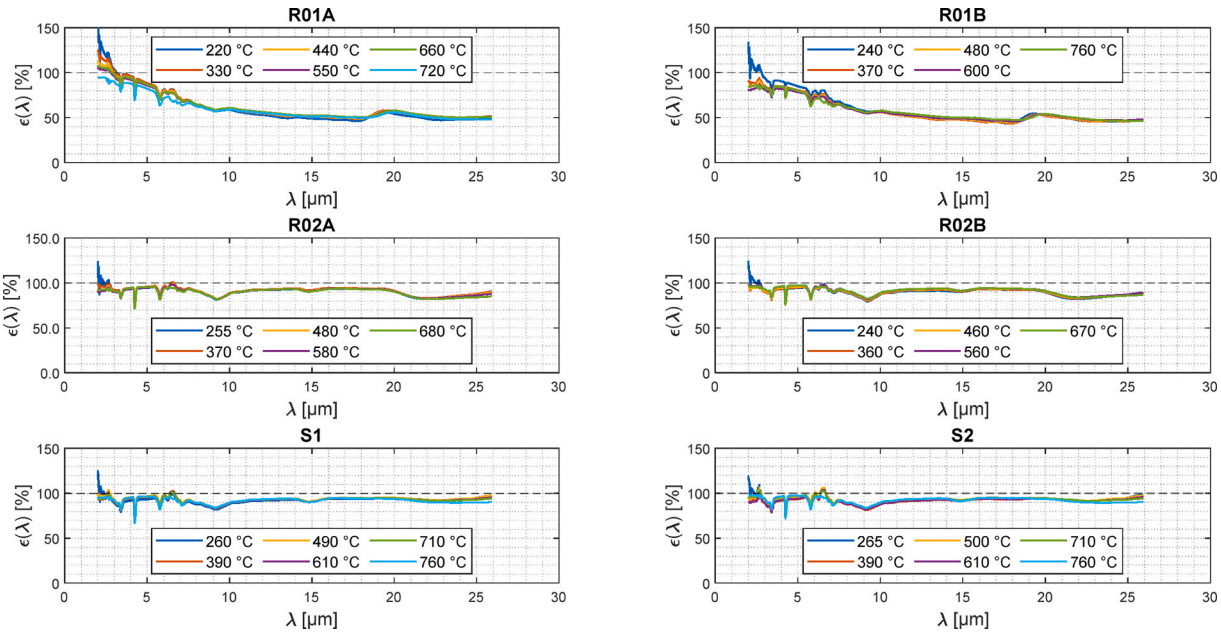

Fig. 10. Spectral measurements recorded for H230 sample coupons at OT from 220 °C to 760 °C by CEA laboratory.

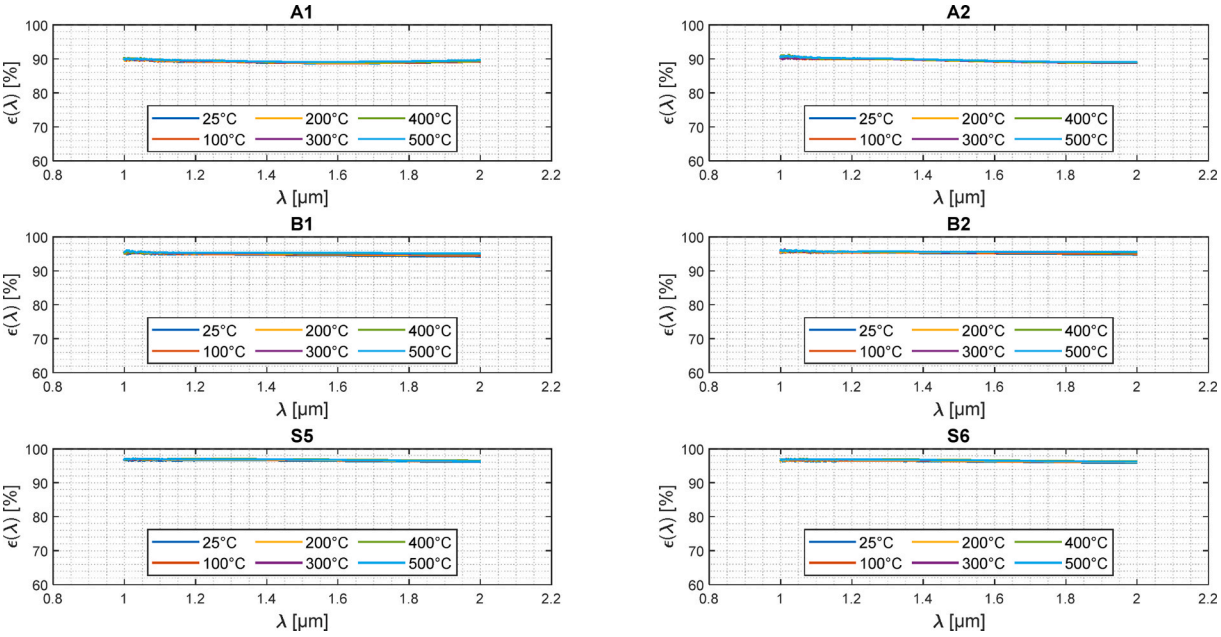

Fig. 11. Spectral measurements recorded for H230 sample coupons from 25 °C to 500 °C by PROMES-CNRS laboratory with the InGaAs detector (1–2 μm).

PROMES-CNRS from 25 °C to 500 °C are respectively shown for the InGaAs and DTGS detectors in Figs. 11 and 12. Spectral measurement for SiC sample coupons are shown Fig. 13 (InGaAs) and Fig. 14 (DTGS). Consistent values are measured with both detectors, without any significant detector noise or atmospheric artefact. For each material, a consistent spectral behaviour is observed among available sample coupons.

For H230 sample coupons, no significant spectral shift is observed from 25 °C to 500 °C (Fig. 11) and a greybody behavior is observed for oxidized and black coated samples from 1 μm to 2 μm. Oxidized H230 (A1/A2) achieves a mean emittance of 90% over this spectral range, while Pyromark 2500 (B1/B2) and the industrial black coating (S5/S6) achieve a mean emittance of 95%. It would thus be possible to discriminate optically oxidized H230 from black coated H230 at short IR wavelengths with an InGaAs infrared detector in IR thermography applications. For DTGS measurements (Fig. 12), weak temperature dependent spectral shifts are observed, H230 sample coupons are however optically stable from 25 °C to 500 °C. Spectral profiles are consistent with previous observations made from Fig. 10.

For SiC sample coupons, no significant spectral shifts are observed from 1 μm to 1.5 μm (Fig. 13), while minor temperature dependent spectral shifts are observed above 2 μm (Fig. 14), especially in the shoulder from 10 μm to 12 μm. SiC behaves nearly as a greybody from 1.5 μm to 9 μm, a selective behavior is then observed from 10 μm to 16 μm. This infrared signature is relevant for longwave IR thermography.

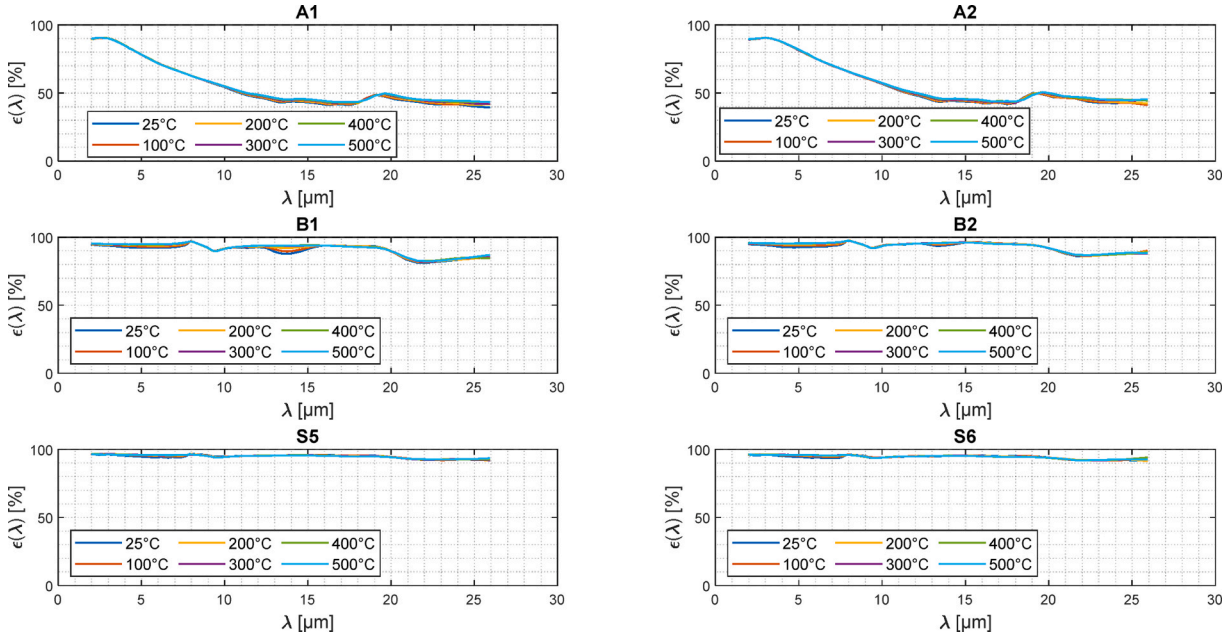

Fig. 12. Spectral measurements recorded for H230 sample coupons from 25 °C to 500 °C by PROMES-CNRS laboratory with the DTGS detector (>2 μm).

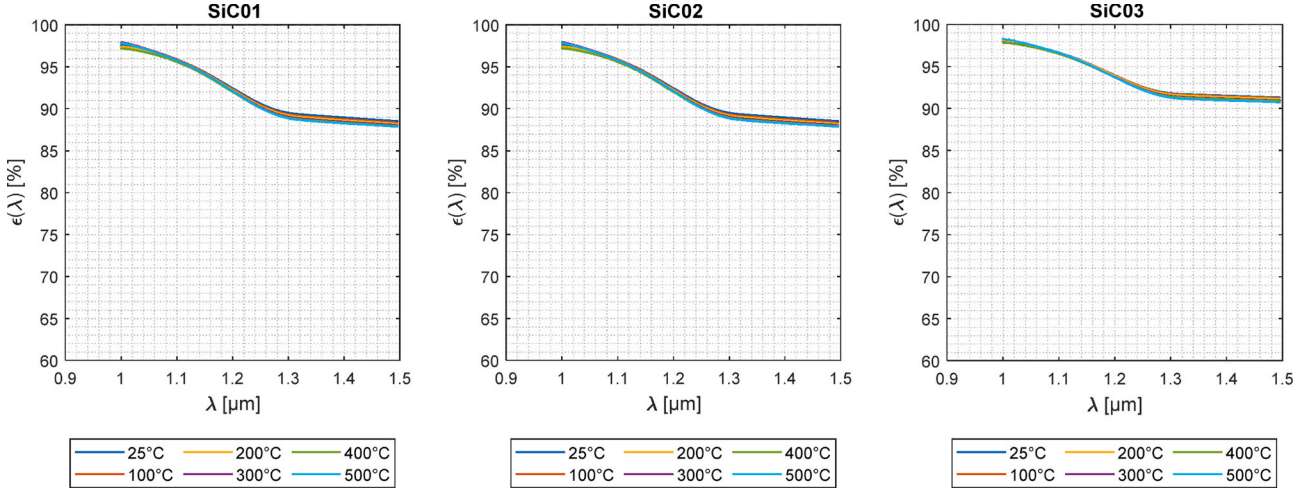

Fig. 13. Spectral measurements recorded for SiC sample coupons from 25 °C to 500 °C by PROMES-CNRS laboratory with the InGaAs detector (1.0-1.5 μm).

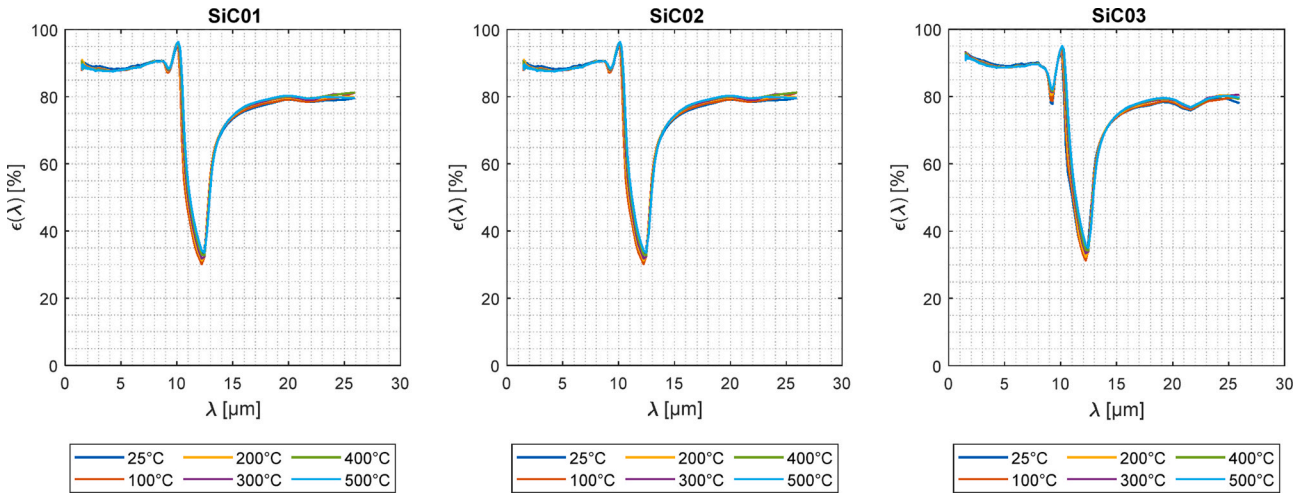

Fig. 14. Spectral measurements recorded for SiC sample coupons from 25 °C to 500 °C by PROMES-CNRS laboratory with the DTGS detector (>1.5 µm).

3.2.3. *MEDIASE setup*

Spectral measurements for H230 sample coupons recorded by PROMES-CNRS at MEDIASE setup from 620 °C to 805 °C are shown in Fig. 15. Weak temperature dependent spectral shifts are observed, with a lower confidence for datasets obtained below 650 °C due to the applied temperature measurement principle [29]. Local artefacts caused by atmospheric absorption bands are observed around 2.7, 4.2 and 5.5 µm, despite the short range between the detector and the measured sample. These artefacts, caused by residual water vapor and carbon dioxide distort locally the emittance spectrum, which locally reaches values above 100%.

The spectral behaviour is consistent for each pair of sample coupons. Spectral profiles are similar to previous measurements in Figs. 10, Figs. 11 and 12 for other experimental setups.

MEDIASE setup allows investigating the influence of the incidence angle thanks to the goniometer optical assembly (Fig. 5). Experimental results are shown in Fig. 16, weighting spectral emittance curves according to (Eq. (12)) from 2 to 14 µm. For H230 sample coupons, a weak angular dependence of thermal emittance is observed from 0° up to 45° ($\Delta\varepsilon_{meas} \sim 1\%$). Above 45°, the deviation is more pronounced. Oxidized H230 or black coated samples can be considered as diffuse surfaces.

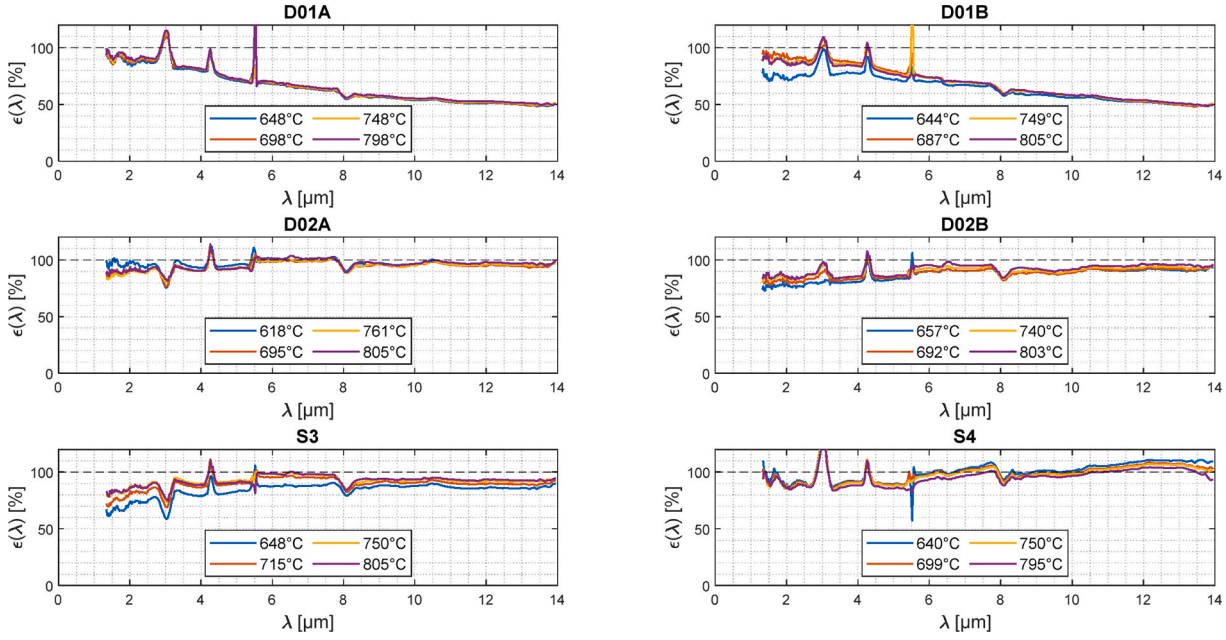

Fig. 15. Spectral measurement datasets recorded at OT from 618 °C to 805 °C by PROMES-CNRS with MEDIASE setup. Samples investigated: D01A, D01B, D02A, D02B, S3, S4.

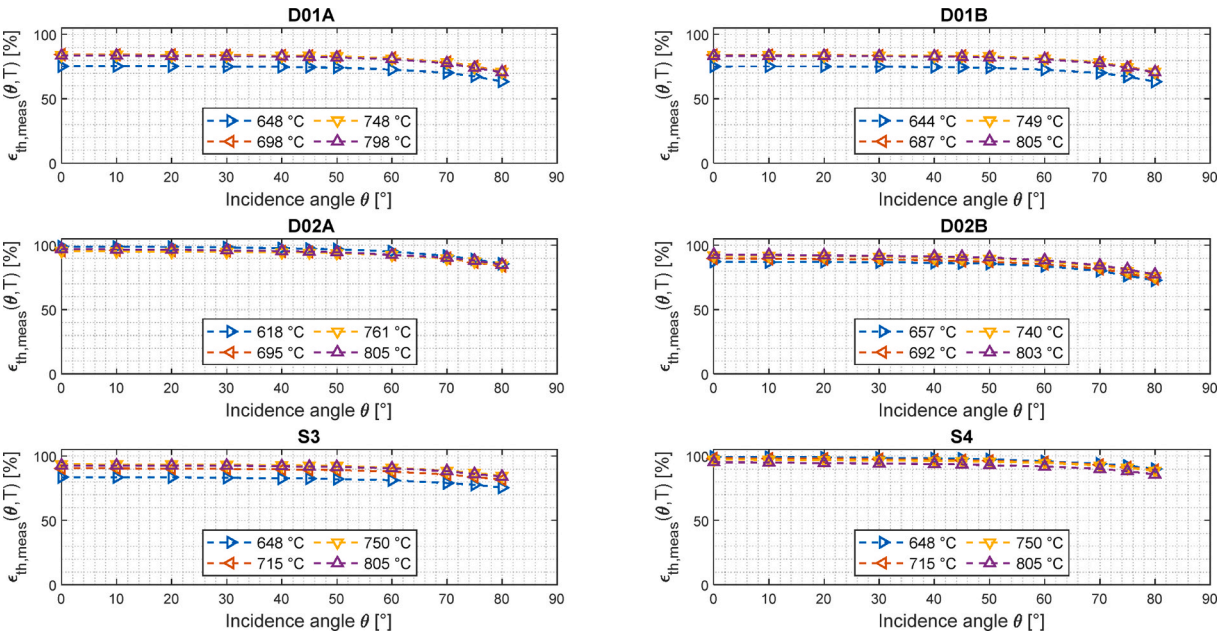

Fig. 16. Influence of incidence angle on thermal emittance $\varepsilon_{th,meas}(T)$ for measurements recorded at OT from 618 °C up to 805 °C by PROMES-CNRS with MEDIASE setup.

3.3. Comparison

Spectral measurements at RT and OT are weighted according to (Eq. (12)) from 2 to 14 μm in order to compare thermal emittance $\varepsilon_{th}(T)$ for H230 and SiC sample coupons at RT and OT. Results are shown in Fig. 17. For RT measurements, $\varepsilon_{th,calc}(T)$ values are averaged for each sample batch and the corresponding standard deviation is shown. For OT measurements, $\varepsilon_{th,meas}(T)$ values are shown for each test samples. In the case of H230 sample coupons, a direct comparison between OT experimental setups is not feasible, as different samples from

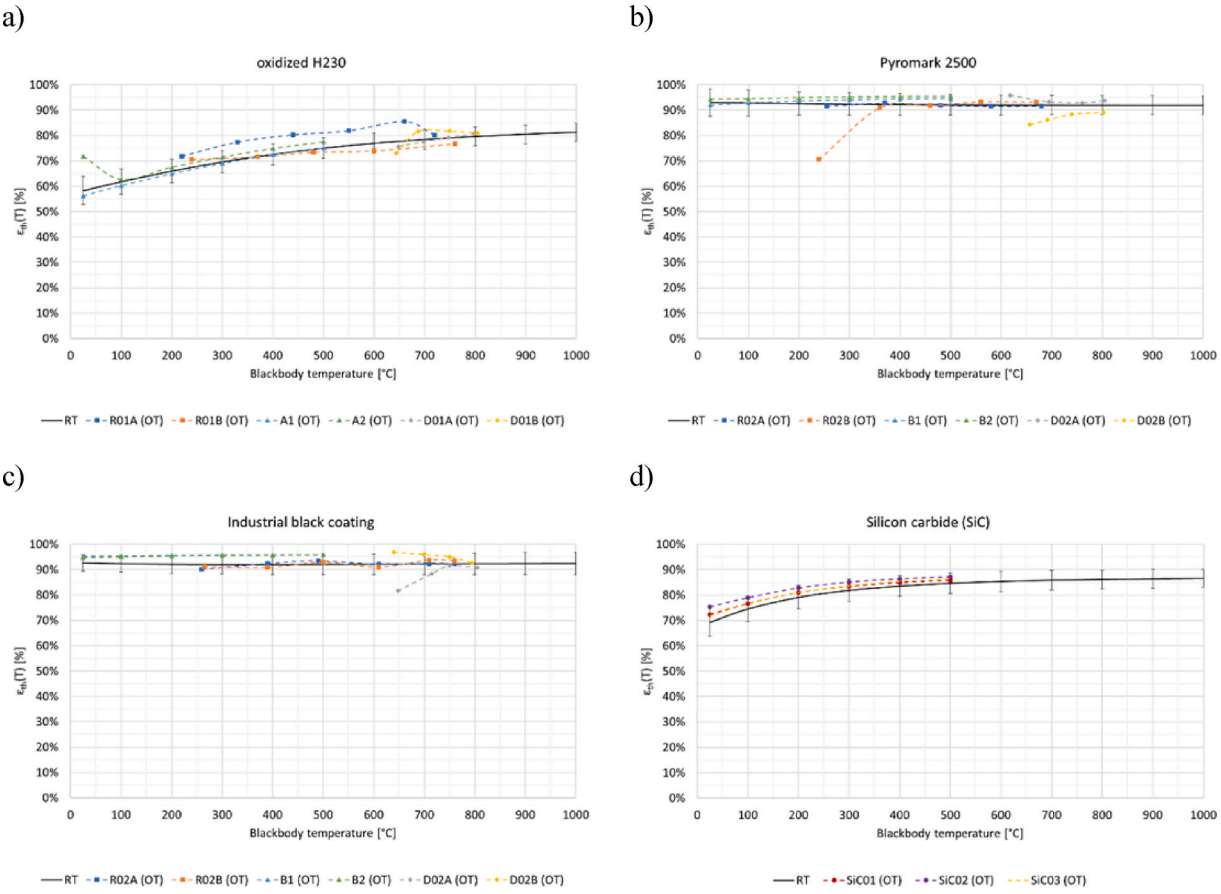

Fig. 17. Comparison of thermal emittance $\varepsilon_{th}(T)$ values for H230 and SiC sample coupons obtained from RT and OT measurements. a) oxidized H230, b) Pyromark 2500, c) Industrial grade black coating, d) SiC sample coupons.

homogeneous batches were measured by each laboratory. Each setup also operated over a different temperature range, with only a partial overlap.

Overall, a fairly consistent agreement is observed between RT and OT measurements for the $\varepsilon_{th}(T)$ indicator, apart for a few outliers in the case of H230 sample coupons, for instance MEDIASE measurements below 650 °C. For oxidized H230, $\varepsilon_{th}(T)$ increases from 55% at RT to nearly 80% at 800 °C (Fig. 17a). For Pyromark 2500 and the industrial black coating, $\varepsilon_{th}(T)$ fluctuates around 90% and a weak temperature dependence is observed (Fig. 17 b & c.). For SiC sample coupons, only PROMES-CNRS OT measurements are exploitable. For this lot, $\varepsilon_{th}(T)$ raises from 70% at RT up to 85% at 500 °C.

4. Conclusion

In this paper, spectral measurements performed by five different European laboratories from room temperature up to 800 °C have been evaluated and compared for relevant receiver materials in Concentrating Solar Thermal applications. Two relevant receiver material substrates were considered Haynes 230 (H230) and Silicon carbide (SiC). H230 was investigated with three different surface finishes i) oxidized, ii) Pyromark 2500, iii) an industrial black coating. Two key figures of merits were analyzed for all samples: solar absorptance α_{sol} and thermal emittance $\varepsilon_{th}(T)$. Solar absorptance α_{sol} was calculated for room temperature measurements over the spectral interval [0.3 – 2.5] μm, while thermal emittance $\varepsilon_{th}(T)$ was calculated for measurements performed at room temperature and operating temperature, over the common spectral range [2–14] μm.

Oxidized H230 sample coupons reached an α_{sol} value of 90.9±1.0%. For samples coupons coated with Pyromark 2500 and the industrial black coating, the α_{sol} value respectively reached 96.3±0.5%, and 97.0±0.4%. Silicon carbide sample coupons reached an α_{sol} value of 93.5±1.1%. Low standard deviations indicated reproducible measurements at room temperature for the α_{sol} figure of merit.

For oxidized H230 sample coupons, the $\varepsilon_{th,calc}(T)$ value derived from room temperature spectral measurements varied from 55% at 25 °C up to 85% at 1000 °C. For Pyromark 2500 and the industrial black coating, the $\varepsilon_{th,calc}(T)$ value lied between 90% and 95%, with a weak temperature dependence. For silicon carbide sample coupons, the $\varepsilon_{th,calc}(T)$ varied from 70% at room temperature up to 87% at 1000 °C. The typical standard deviation among participating laboratories is about 3%. Consistent $\varepsilon_{th,calc}(T)$ values were obtained for room temperature spectral measurements, with a higher standard deviation in comparison to the solar absorptance α_{sol}.

For both figures of merit α_{sol} and $\varepsilon_{th,calc}(T)$, all absolute Z-score values were lower than 2, i.e. the intercomparison of both figures of merit at room temperature could be interpreted as statistically satisfactory according to ISO 13528.

Spectral measurements at operating temperature were performed by two laboratories (CEA and PROMES-CNRS) with three different experimental setups. Thermal emittance $\varepsilon_{th,meas}(T)$ values obtained from spectral measurements performed at operating temperature up to 800 °C were overall consistent within a few percentage points in comparison to thermal emittance $\varepsilon_{th,calc}(T)$ values obtained from spectral measurements at room temperature, despite a few outliers.

CRediT authorship contribution statement

Simon Caron: Writing – review & editing, Writing – original draft, Visualization, Methodology, Investigation, Conceptualization. **Meryem Farchado:** Writing – review & editing, Investigation. **Gema San Vicente:** Writing – review & editing, Investigation. **Angel Morales:** Writing – review & editing, Investigation. **Jesus Ballestrín:** Writing – review & editing, Investigation. **Maria Joao Carvalho:** Writing – review & editing, Investigation. **Soraia Pascoa:** Writing – review & editing, Investigation. **Estelle le Baron:** Writing – review & editing, Investigation. **Angela Disdier:** Investigation, Writing – review & editing. **Emmanuel Guillot:** Writing – review & editing, Investigation. **Christophe Escape:** Writing – review & editing, Investigation. **Jean-Louis Sans:** Writing – review & editing, Investigation. **Yaniv Binyamin:** Writing – review & editing. **Mubeen Baidossi:** Writing – review & editing. **Florian Sutter:** Writing – review & editing, Project administration, Funding acquisition. **Marc Röger:** Writing – review & editing, Project administration, Funding acquisition. **Francisco Manzano-Agugliaro:** Writing – review & editing, Visualization, Supervision.

Declaration of competing interest

The authors declare that they have no known competing financial interests or personal relationships that could have appeared to influence the work reported in this paper.

Data availability

Data will be made available on request.

Acknowledgments

This work has received funding from the European Union's Horizon 2020 Research and Innovation Program under grant agreement n° 823802 (EU SFERA-III). The industrial black coating was provided within the project TubeMon, funded by the (SOLAR-ERA.Net European network (project ID 50).

References

[1] International Renewable Energy Agency (IRENA), Solar energy. 2020. https://www.irena.org/Energy-Transition/Technology/Solar-energy. (Accessed 24th November 2023).
[2] World Bank, Concentrating solar power: clean power on demand 24/7 (2021) 65. https://pubdocs.worldbank.org/en/849341611761898393/WorldBank-CSP-Report-Concentrating-Solar-Power-Clean-Power-on-Demand-24-7-FINAL.pdf. (Accessed 24th November 2023).
[3] German Aerospace Center (DLR) Institute of Solar Research, Solar thermal powerplants: heat, electricity and fuels from concentrated solar power 27 (2021). https://www.dlr.de/sf/en/PortalData/73/Resources/dokumente/publikationen_medien/dlr_und_sf/Study_Solar_thermal_power_plants_DLR_2021-05.pdf. (Accessed 24th November 2023).
[4] C.K. Ho, B.D. Iverson, Review of high-temperature central receiver designs for concentrated solar power, Renew. Sustain. Energy Rev. 29 (2014) 835–846, https://doi.org/10.1016/j.rser.2013.08.099.
[5] C.K. Ho, Advances in central receivers for concentrating solar applications, Sol. Energy 152 (2017) 38–56, https://doi.org/10.1016/j.solener.2017.03.048.
[6] A.L. Avila-Marin, Volumetric receivers in solar thermal power plants with central receiver system technology: a review, Sol. Energy (5) (2011) 891–910, https://doi.org/10.1016/j.solener.2011.02.002.
[7] L. Noc, E. Sest, G. Kapun, F. Ruiz-Zepeda, Y. Binyamin, F. Merzel, I. Jerman, High solar-absorptance CSP coating characterization and reliability testing with isothermal cyclic loads for service-life prediction, Energy Environ. Sci. 12 (2019) 1679–1694, https://doi.org/10.1039/C8EE03536A.
[8] J.F. Torres, K. Tsuda, Y. Murakami, Y. Guo, S. Hosseini, C.A. Asselineau, M. Taheri, K. Drewes, A. Tricoli, W. Lipiński, J. Coventry, Highly efficient and durable solar thermal energy harvesting via scalable hierarchical coatings inspired by stony corals, Energy Environ. Sci. 15 (2022) 1893–1906, https://doi.org/10.1039/D1EE03028K.
[9] A. Boubault, C.K. Ho, A. Hall, T.N. Lambert, A. Ambrosini, Durability of solar absorber coatings and their cost-effectiveness, Sol. Energy Mater. Sol. Cell. 166 (2017) 176–184, https://doi.org/10.1016/j.solmat.2017.03.010.
[10] S. Caron, J. Garrido, J. Ballestrin, F. Sutter, M. Röger, F. Manzano-Agugliaro, A comparative analysis of opto-thermal figures of merit for high temperature solar thermal absorber coatings, Renew. Sustain. Energy Rev. 154 (2022) 21, https://doi.org/10.1016/j.rser.2021.111818, 111818.
[11] S. Caron, L. Herding, Y. Binyamin, M. Baidossi, Y. Vinietsky, A. Morales, C. Hildebrandt, R. Reoyo-Prats, O. Faugeroux, A. Agüero, S. Rodriguez, F. Sutter, M. Röger, F. Manzano-Agugliaro, A laboratory intercomparison of solar absorptance and thermal emittance measurements at room temperature, Sol. Energy Mater. Sol. Cell. 238 (2022) 15, https://doi.org/10.1016/j.solmat.2022.111579, 111579.
[12] C.K. Ho, A.R. Mahoney, A. Ambrosini, M. Bencomo, A. Hall, T.N. Lambert, Characterization of Pyromark 2500 paint for high-temperature solar receivers, J. Sol. Energy Eng. 136 (1) (2014) 4, https://doi.org/10.1115/1.4024031, 014502.
[13] E. Le Baron, O. Raccurt, P. Giraud, M. Adier, J. Barriga, B. Diaz, P. Echegut, D. De Sousa Meneses, C. Capiani, D. Sciti, A. Soum-Glaude, C. Escape, I. Jerman, G.

A. Lopez, T. Echaniz, M.J. Tello, F. Matino, A. Maccari, L. Mercatelli, E. Sani, Round Robin Test for the comparison of spectral emittance measurement apparatuses, Sol. Energy Mater. Sol. Cell. 191 (2019) 476–485, https://doi.org/10.1016/j.solmat.2018.11.026.

[14] I. Setien-Fernandez, T. Echaniz, L. Gonzalez-Fernandez, R.B. Perez-Saez, E. Cespedes, J.A. Sanchez-Garcia, L. Alvarez-Fraga, R. Escobar Galindo, J. M. Albella, C. Prieto, M.J. Tello, First spectral emissivity study of a solar selective coating in the 150-600°C temperature range, Sol. Energy Mater. Sol. Cell. 117 (2013) 390–395, https://doi.org/10.1016/j.solmat.2013.07.002.

[15] T. Echaniz, I. Setien-Fernandez, R.B. Perez-Saez, C. Prieto, R. Escobar Galindo, M. J. Tello, Importance of the spectral emissivity measurements at working temperature to determine the efficiency of a solar selective coating, Sol. Energy Mater. Sol. Cell. 140 (2015) 249–252, https://doi.org/10.1016/j.solmat.2015.04.009.

[16] I. Gonzalez de Arrieta, T. Echaniz, R. Fuente, E. Rubin, R. Chen, J.M. Igartua, M. J. Tello, G.A. Lopez, Infrared emissivity of copper-alloyed spinel black coatings for concentrated solar power systems, Solar Energy Materials and Solar Cells, Sol. Energy Mater. Sol. Cell. 200 (2019) 9, https://doi.org/10.1016/j.solmat.2019.109961, 109961.

[17] D. Hernandez, G. Olalde, J.M. Gineste, C. Gueymard, Analysis and experimental results of solar-blind temperature measurements in solar furnaces, J. Sol. Energy Eng. 126 (1) (2004) 645–653, https://doi.org/10.1115/1.1636191.

[18] A. Marzo, J. Ballestrin, J. Barbero, I. Cañadas, J. Rodríguez, Solar blind pyrometry not relying on atmospheric absorption bands, Sol. Energy 107 (2014) 415–422, https://doi.org/10.1016/j.solener.2014.04.031.

[19] M. Balat-Pichelin, J.-L. Sans, E. Bêche, L. Charpentier, A. Ferrière, S. Chomette, Emissivity at high temperature of Ni-based superalloys for the design of the solar receiver for future tower power plants, Sol. Energy Mater. Sol. Cell. 227 (2021) 12, https://doi.org/10.1016/j.solmat.2021.111066, 111066.

[20] M. Balat-Pichelin, A. Bousquet, Total hemispherical emissivity of sintered SiC up to 1850 K in high vacuum and in air at different pressures, J. Eur. Ceram. Soc. 38 (10) (2018) 3447–3456, https://doi.org/10.1016/j.jeurceramsoc.2018.03.050.

[21] N. Azzali, M. Meucci, D. Di Rosa, L. Mercatelli, L. Silvestroni, D. Sciti, E. Sani, Spectral emittance of ceramics for high temperature solar receivers, Sol. Energy 222 (2021) 74–83, https://doi.org/10.1016/j.solener.2021.05.019.

[22] J. Coventry, P. Burge, Optical properties of Pyromark 2500 coatings of variable thicknesses on a range of materials for concentrating solar thermal applications, AIP Conf. Proc. 8 (2017), https://doi.org/10.1063/1.4984355,1850:030012.

[23] A. Ambrosini, A. Boubault, C.K. Ho, L. Banh, J.R. Lewis, Influence of application parameters on stability of Pyromark 2500 receiver coatings, AIP Conf. Proc. 8 (2019), https://doi.org/10.1063/1.5117514,2126:030002.

[24] S. Caron, J. Garrido, E. Setien, R. Harzallah, L. Noc, I. Jerman, M. Röger, F. Sutter, Forty shades of black: a benchmark of high temperature sprayable black coatings applied on Haynes 230, AIP Conf. Proc. 10 (2020), https://doi.org/10.1063/5.0028773,2303:1560007.

[25] S. Hosseini, J.F. Torres, M. Taheri, A. Tricoli, W. Lipiński, J. Coventry, Long-term thermal stability and failure mechanisms of Pyromark 2500 for high-temperature solar thermal receivers, Sol. Energy Mater. Sol. Cell. 246 (2022), 111898, https://doi.org/10.1016/j.solmat.2022.111898.

[26] N. Martínez, M. Lopez-Herraiz, A. Rico, C.J. Múnez, P. Poza, Influence of different thermal degradation processes on the optical property of Pyromark-2500, Sol. Energy 253 (2023) 58–72, https://doi.org/10.1016/j.solener.2023.02.004.

[27] P. Giraud, J. Braillon, C. Delord, O. Raccurt, Development of optical tools for the characterization of selective solar absorber at elevated temperature, AIP Conf. Proc. 1734 (2016), 130008, https://doi.org/10.1063/1.4949218.

[28] Infrared System Development Corporation, IR 563/301 Blackbody system. https://www.infraredsystems.com/Products/blackbody563.html. (Accessed 24th November 2023).

[29] D. Hernandez, J.L. Sans, A. Netchaieff, P. Ridoux, V. Le Sant, Experimental validation of a pyroreflectometric method to determine the true temperature on opaque surface without hampering reflections, Measurement 42 (6) (July 2009) 836–843, https://doi.org/10.1016/j.measurement.2009.01.012.

[30] Ci Systems, SR-5000N spectroradiometer. https://www.ci-systems.com/SR-5000N-Spectroradiometer. (Accessed 24th November 2023).

[31] ASTM International, Standard Tables for Reference Solar Spectral Irradiances: Direct Normal and Hemispherical on 37◦ Tilted Surface (2020) 21, https://doi.org/10.1520/G0173-03R20. ASTM G173:2012.

[32] International Standard Organization, statistical methods for use in proficiency testing by interlaboratory comparison, ISO 13528:2015 (2015) 89. https://www.iso.org/standard/56125.html.